XXI IMEKO World Congress "Measurement in Research and Industry"
August 30 – September 4, 2015, Prague, Czech Republic

PHOTOMETRIC STEREO SYSTEM FOR DETAILED ANALYSIS OF MATERIAL SURFACES

Marja Mettänen, Joonas Melin, Heimo Ihalainen

Department of Automation Science and Engineering, Tampere University of Technology, Tampere, Finland,
marja.mettanen@tut.fi, joonas.melin@tut.fi, heimo.ihalainen@tut.fi

Abstract – This paper describes a photometric stereo system for the measurement of surface topography. The system provides versatile experimental possibilities due to movable multicolor LEDs, movable camera, and a traveling (xy-) table for the sample. We introduce our measurement setup and present analysis of its performance. Our topography maps correlate well with the contact profilometry reference map, and reveal different details of the surfaces depending on the illumination wavelength and pixel size.

Keywords: surface topography, photometric stereo

1. INTRODUCTION

Photometric stereo provides a fast non-contact method for estimating the local surface orientations on a selected area of the surface. The orientation information, expressed as surface normals, can be reconstructed into a surface topography map to investigate the shape of the surface, in various size scales. Photometric stereo is widely used in computer graphics for surface analysis and reconstruction.

The photometric stereo setup consists of a stationary camera and light sources in various angles. Photographs of the sample are taken with varying illumination directions, typically using one light source at a time, while the sample lies still, e.g., on table. The inference of the surface orientation (i.e., gradients) from these intensity images relies on the assumption that the intensity in a point depends directly on the gradient values at that point, given the imaging geometry and additional assumptions about the surface reflection model. More precisely, the basic assumption in photometric stereo systems is often the one pioneered by Woodham [1], stating that the surface normal vectors can be uniquely determined by least-squares when at least three images have been taken with known illumination directions, and when the surface is Lambertian.

In practice, the objects under investigation very rarely have purely Lambertian surface reflectance. Common non-Lambertian disturbances include specular highlights, cast and self-shadows and image noise. There are two approaches to deal with these problems: adopting a reflectance map model that is more versatile than Lambertian (e.g., [2, 3]), or identifying the points in which the data is doubtful and applying a special procedure on them [4, 5, 6, 7]. Argyriou and Petrou [4] present iterative surface reconstruction in the presence of self and cast shadows and highlights, assuming Lambertian reflection model in the non-problematic pixels. Alldrin et al. [5] present a photometric stereo method designed for surfaces with spatially-varying BRDFs (bidirectional reflectance distribution functions). Ikehata et al. [7] propose a hierarchical Bayesian approximation to estimate surface normals and simultaneously separating the non-Lambertian corruptions. A moderately recent overview of the various techniques proposed for detecting and correcting the errors in the estimated surface normals can be found in [6]. The examples typically presented in these computer-vision related articles contain macroscopic objects such as statues or human faces.

We have designed and built a photometric stereo imaging system that enables versatile practical experiments on the estimation of surface normals of various materials. Our focus is on applying photometric stereo to the small-scale surface analysis of nominally planar objects. Our history in this area is in the measurement of paper surface topography, which is important for printability (e.g., [8, 9]). We intend to continue with paper, cardboard and other types of fibrous, complicated surfaces, whose surface topography largely affects their end-use properties. The surface topography of paper products has typically been measured with scanning profilometers (e.g., [10]) but those have the problem that the measurement takes very long - from several minutes to hours. A camera-based measurement system, such as a photometric stereo approach, can acquire detailed images of paper even on-line on a paper machine, although the paper travels at the speed of 120 km/h.

Apart from the dermatology application presented recently by Sohaib et al. [11], it is uncommon to find photometric stereo applied to very small-scale surface analysis, i.e., pixel sizes as small as a few micrometers and details as small as the 20-30 µm thick fibres in paper. In addition, Granberg et al. [12] demonstrate that the diffuse reflectance from fiber-containing surfaces is nonuniform, and computer vision models assuming that the reflectance distribution is made up of a specular and a Lambertian component often fail for fiber-containing surfaces [13]. Therefore, to get a realistic view of the applicability of photometric stereo on the small-scale surface analysis of various fibrous products, the basic photometric stereo approach needs to be updated by appropriate corrections of the non-Lambertian effects that occur on fibrous surfaces in micro-scale. The long-term aim of our work is to investigate the non-Lambertian effects, try some of the already proposed error corrections to them, and possibly develop a

new error correction procedure that makes use of the optical properties of fibres and stochastic fibrous structures.

In this paper, we introduce our photometric stereo based setup designed for the measurement of surface topography from paper and other planar targets that exhibit micro-scale roughness. After the description of the system, we present analysis of its performance through the inspection of a small-scale dot grid target. We then compare our surface topography maps, in three different resolutions, with a reference map that has been measured with a contact profilometer. We also summarize our latest observations about the topography maps of paper samples imaged with red, green, and blue illumination. Finally we discuss the future of this research and present conclusions.

2. THE MEASUREMENT SYSTEM

The photometric stereo setup consists of a camera that is situated right on top of the sample (i.e., viewing direction $\sigma = 0°$), and light sources in slant angles; see Fig. 1. The polar angle, σ, is the angle between the viewing direction and the light source, and the azimuth angle, τ, is the angle between the x-axis of the image and the projection of the illumination vector onto the xy-plane. In our setup, basically four images are taken of the sample with different illumination directions; the polar angle, σ, of the illumination is constant, and the azimuth angle, τ, gets four values that are 90° apart from each other. More illumination directions are available through the movement of the LED light sources up and down, and in the azimuthal direction.

2.1. Overview of the measurement system

We have designed the measurement system to be robust and capable of performing various kinds of measurements without the need to rebuild the system. The subsystems of the measurement setup are shown in Fig. 2. The system lies on a pneumatically stabilized table which decouples the frame from the floor, which is necessary to prevent vibrations from affecting the camera. The frame itself is constructed from an aluminium profile to make the configuration of the measurement system stiff but easy to modify if needed. The aluminium profiles have been upholstered by black felt cloth to reduce light reflections inside the measurement frame. In addition, the frame is covered from outside with a black felt cloth to prevent stray light.

2.2. Movable axes

The measurement system consists of several axes that can be translated or rotated. The translational axes are for moving the sample in the horizontal plane (xy-plane), elevating the lights in the vertical (z-) direction and for moving the camera in the vertical direction, e.g., for focusing purposes. Two rotational axes are assigned to moving the light fixtures in a horizontal plane around the sample. The other rotational axis is in front of the lights to make it possible to automatically change filters and polarizers for the lights.

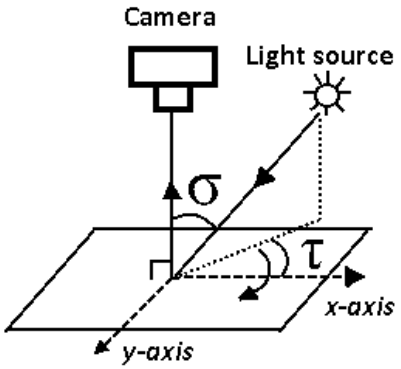

Fig. 1. The principle of photometric stereo.

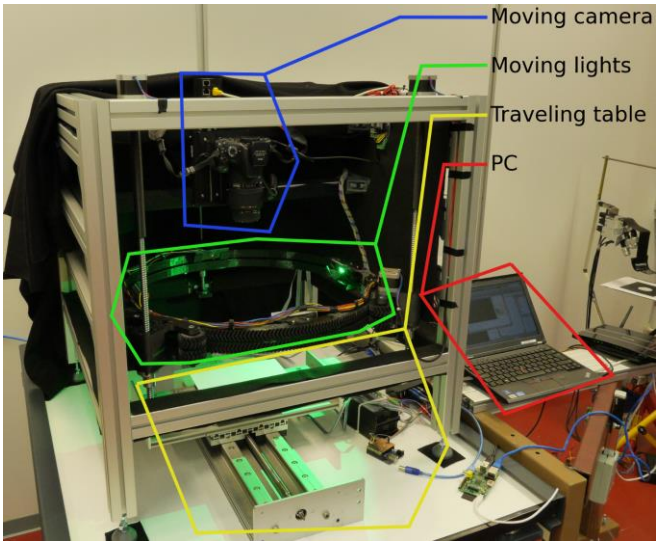

Fig. 2. The basic components of the measurement system.

2.3. Camera and lights

The photographs are captured using a digital systems camera (Canon EOS 550D), and a 105 mm macro lens from Sigma, or Canon MP-E 65 mm macro lens capable of up to 5-fold magnification. The sensor of the camera has 18 megapixels in an area of 22.3 mm by 14.9 mm. With 1:1 magnification this produces pixels of size 4.3 µm by 4.3 µm.

The lights are 10 W LED lights. We chose RGB LED lights with two green elements and one element for red and one for blue so that we would not have to necessarily rely on the bayer matrix of the camera to distinguish between different wavelengths. The nominal wavelengths of the red, green, and blue channels of our current LEDs are 625 nm, 523 nm and 460 nm, respectively.

The light fixtures are designed as 470 mm diameter gears which are supported from three points. These three points are further attached to a ball screw that moves the whole fixture in the vertical direction. Idler gears prevent the attachment points from rotating during the movement of the vertical axis. The gears on the light fixtures have been printed with a double helical profile to eliminate the need for supporting structures. All the movements of the measurement system are implemented with stepper motors.

2.4. Communication

As the measurement system consists of several subsystems, we simplify the communication with the use of a master device for the serial port devices, as the operating system on the processing computer is not capable of persistent device naming. Our solution is to pass through data from TCP/IP ports to serial ports through a Linux based machine.

2.5. Computation of surface topography

The basic principle of solving the surface normal at each pixel is based on [1]. Briefly, the surface normals are estimated by the least-squares solution of a linear set of equations, relying on the Lambertian surface reflection model in which the light intensity, I, observed in a point depends on surface albedo, ρ, surface normal vector, $\mathbf{n}$, and illumination direction, $\mathbf{l}$, $I = \rho \boldsymbol{n}^T \boldsymbol{l}$.

Given m images, each taken with a unique illumination direction, an individual pixel is associated with m intensities (I becomes a vector of length m), and the illumination directions are collected into a 3-by-m matrix. The scaled surface normal, $\rho\mathbf{n}$, can thus be solved for each pixel.

The lights in our system are not very far away from the target surface, and hence the illumination direction and intensity depend on the pixel location. Therefore, prior to computing the surface normal estimates, the illumination pattern is compensated by taking a set of illumination calibration images, using a flat target of the same color as the sample under investigation, and determining the pattern from these images. Our method resembles that of Sun et al. [14] in the illumination compensation, except that we prefer to fit a second order 2D polynomial to each illumination calibration image and divide our sample image with this polynomial, instead of dividing the sample image with the calibration image directly, as in Eq. (5) in [14]. The polynomial approach is free from spurious samples such as potential dead pixels.

After estimating the surface normal for each pixel, the gradients are computed as $gx = \mathbf{n}_1/\mathbf{n}_3$ and $gy = \mathbf{n}_2/\mathbf{n}_3$. Finally, the gradient fields are integrated to reconstruct the surface topography estimate [15].

3. EXPERIMENTS AND RESULTS

Through the imaging and investigation of various planar samples, such as glass, aluminium oxide, and paper, we have been able to make sure that the photometric stereo system performs as expected. The construction has been found very stable and the images are clear.

We have inspected the quality of the imaging system through images of a 25 mm by 25 mm distortion target by Edmund Optics. The glass target contains a grid of black dots of diameter 62.5 µm, and 125 µm apart from each other. We have used both the Sigma 105 mm macro objective and the Canon MP-E 65 mm macro objective with up to 3-fold magnification, and captured images of the distortion target in red, green, blue and white illumination. The aperture setting was f/7.1. From the images, it is possible to estimate both the point spread function (PSF) and the geometric distortions induced by the imaging system. An estimate of the PSF is needed when integrating the gradient fields. The top part of Fig. 3 presents an image of one dot, cropped from the Bayer-separated green channel of a photograph in which the MP-E objective is in use and the pixel size is 2.8 µm. It shows that even with the magnifying objective, the impulse response of the optical system is very sharp.

The latter part of Fig. 3 illustrates the geometric distortions in the same image. The presented corner is the most distorted part of the image, however, the observed dot locations (magenta markers) are at most 2.5 pixels away from the regular grid positions (yellow markers). The Levenberg-Marquardt method was used to fit radial distortion parameters [16] between the regular and observed locations of the black dots, and this reduced the root mean square error of the dot locations from 1.0 pixels to 0.5 pixels. In a similar experiment with the 1:1 objective (Sigma 105 mm), the radial distortion estimation reduced the RMS error of the dot locations from 1.5 pixels to 0.9 pixels.

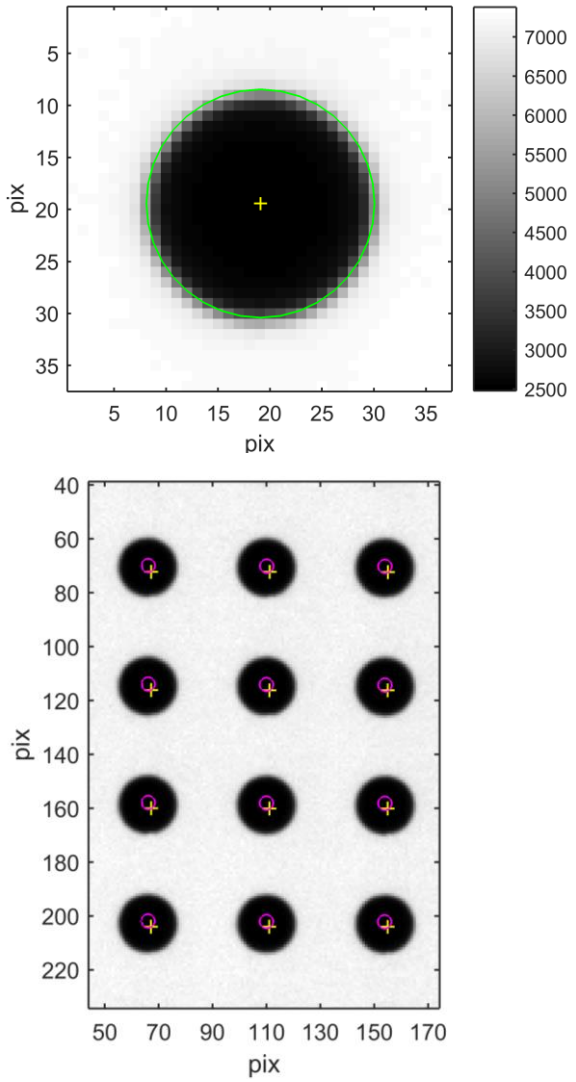

Fig. 3. (Top:) Average of four dot images, taken with the Canon MP-E 65 mm macro objective. The true diameter of the dot is 62.5 µm. The theoretical edge of the dot is presented by the green line and the center of the dot by the yellow marker. (Bottom:) A close-up of the most distorted corner of an image of the distortion target. The yellow markers denote the theoretical dot locations and the magenta markers denote the true locations in the distorted image.

To compare the surface topography reconstructions computed from our photometric stereo images with a known

reference surface topography, we have measured the surface of a piece of white aluminium oxide with a Dektak XT surface profilometer. It constructs a surface topography map of the target by scanning the surface with a mechanical (i.e., touching) stylus. The pixel size in the reference measurement is 2.5 µm by 2.0 µm. From the same area, we have measured the surface topography with photometric stereo (PS) using three different pixel sizes: 6.1 µm, 3.0 µm and 1.4 µm (square shaped pixels). We have then registered the PS based surface reconstructions with the reference topogaphy map with sub-pixel accuracy [17]. Table 1 shows the point-wise correlation coefficients between the PS based surface topography maps and the reference surface topography after spatial alignment.

Table 1. Photometric stereo (PS) measurements compared with the reference surface topography.

Pixel size	Polar angle	Corr.coeff. (PS vs. Ref.)
6.1 by 6.1 µm	75°	0.83
3.0 by 3.0 µm	74°	0.84
1.4 by 1.4 µm	60°/70°	0.71

Fig. 4 shows the reference surface topography map and illustrates the areas from which the PS measurements were made. The bottom part of Fig. 4 shows profile lines extracted from the aligned topography maps.

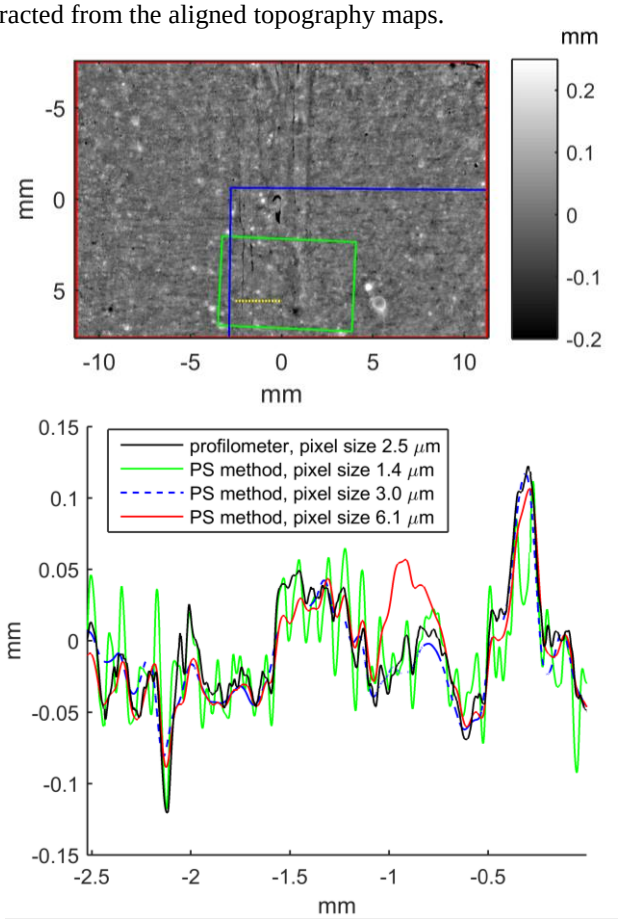

Fig. 4. (Top:) Surface topography map of aluminium oxide, measured with the contact profilometer. The rectangles denote the positions of the spatially aligned PS measurements in resolutions 6.1 µm (red), 3.0 µm (blue) and 1.4 µm (green). The yellow dotted line denotes the position of the profile line plotted in the lower subfigure.

The photometric stereo measurement of the aluminium oxide seem to capture the surface topography moderately, but there are some errors as well. The resolution in PS measurements with 6.1 µm and 3.0 µm pixel sizes (the red and blue curves, respectively) is not high enough to capture all the details of the surface that were observed by the contact profilometer. There is also a gross error in the red curve, showing as a bump at around -1 mm. It may have been caused by shadowing, as the illumination polar angle was as large as 75°. The highest resolution PS measurement, presented by the green curve, is somewhat restless, but it captures the extreme peaks and valleys of the reference profile quite well. Since it has been reconstructed as a combination of 60° and 70° illumination polar angles, it is expected to be less prone to highlights, shadows, and other non-Lambertian effects than the other versions. On the other hand, the very small pixel size exposes this measurement to exactly those kind of problems.

All the comparisons shown above have been made using green illumination and green color channels of the PS based topography maps. The correlation coefficients, such as those presented in Table 1, showed little variation when the topography maps were computed from red or blue illuminated photographs. The colors play a larger role when the samples have a less dense surface. A brief description of an experiment with a set of paper samples will therefore close this section.

We have imaged the surfaces of a coated white paper, grocery bag, brown kraft paper and a topliner with the 1:1 magnification, using red, green, and blue illumination. Three polar angles, namely 55°, 65° and 75°, and 12 azimuth angles, have been applied in this data set. Light scattering and reflectivity of the fibres and fillers in paper depend on illumination wavelength [18]. Furthermore, the hollow wood fibres transport light and occasionally make it enter the paper surface in one point and exit at another point. We have examined the dependence of the surface topography reconstructions on the wavelength of light by computing the point-wise correlation coefficients between the gradient images estimated from various 4-light configurations. The gradient image is more suitable for this purpose than the topography map, because the latter is blurred by the integration. At each illumination polar angle, there are three 4-light sets whose azimuthal configurations are 30° apart from each other. Computing the correlations pair-wise from these sets produces three correlation coefficients, and averaging these three gives the results presented in Table 2.

Table 2. Average point-wise correlation coefficients between gradient images estimated from 4-light configurations.

Gradient direction	Polar angle	Red	Green	Blue
x	55°	0.73	0.82	0.83
	65°	0.79	0.84	0.85
	75°	0.84	0.87	0.87
y	55°	0.70	0.79	0.81
	65°	0.75	0.82	0.83
	75°	0.81	0.84	0.85

The correlation coefficients between the gradient images are clearly lower than 1, which means that the estimated 4-light gradients depend on the illumination direction. It is also

seen that the blue illumination (i.e., the shortest wavelength) produces the most similar gradient images while the red illumination results in the least similar gradients. This is in line with the fact that longer wavelengths propagate further into the structure of the paper while shorter wavelengths reflect closer to the surface [18].

Finally, Fig. 5 presents an example of the x-gradients of a rough brown kraft sample, estimated from 4-light, 12-light, and 36-light illumination configurations. The first two have an illumination polar angle of 65° while the last one is the combination of all of the polar and azimuth angles applied in this experiment. The illumination color is blue.

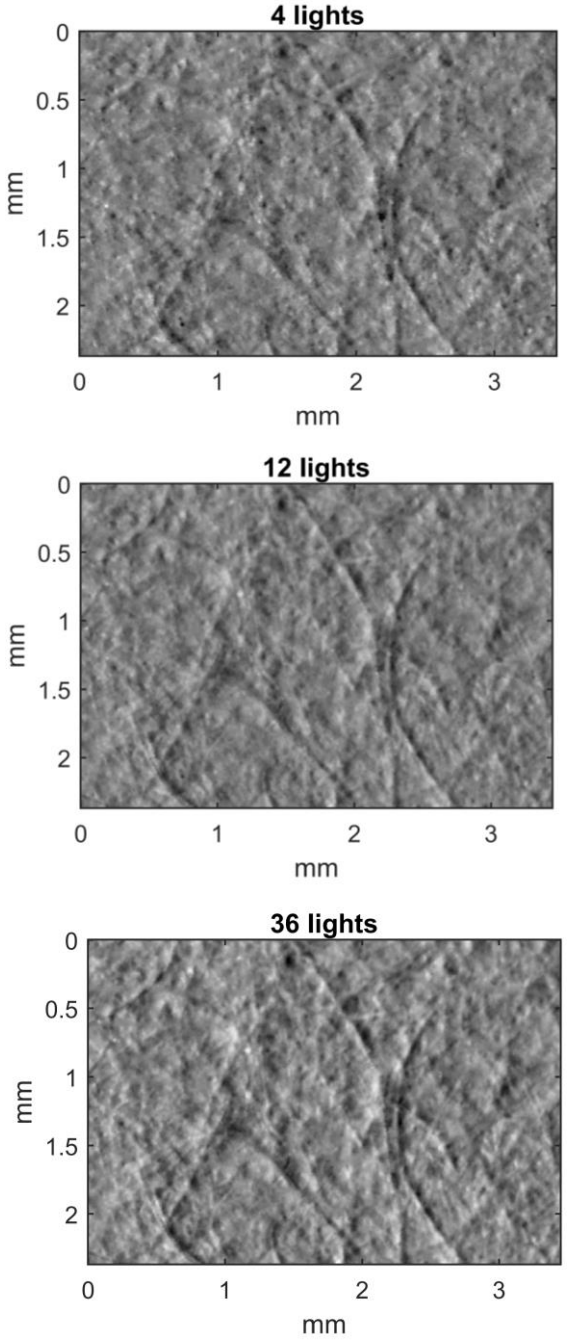

Fig. 5. Close zoom of the x-gradient images of a kraft paper sample illuminated with four blue lights at polar angle 65° (top), twelve lights at polar angle 65° (middle), and 36 lights (bottom; a combination of polar angles 55°, 65° and 75°).

The gradient images shown in Fig. 5 imply that combining several illumination directions improves the gradient estimate by revealing more details from the surface and reducing spurious gradient values such as the "hole" in the 4-light gradient at the crossing of two fibres (approximately $x = 2.2$; $y = 1.3$ mm).

4. DISCUSSION

There is obviously work to be done with the computation algorithms to reduce errors in surface normals due to the non-Lambertian effects. As shown by the example in Fig. 5, steep gradients, self-shadowng, and specular reflections can result in considerable uncertainty in the gradient estimation when the number of illumination directions is small.

A large part of our focus so far has been on the mechanical design, and on the assessment of the illumination conditions inside the measurement frame. For instance, there was a seemingly significant extra source of light that was formed by the bright aluminium cooling plates of the LEDs. However, painting the plates with matte black was found - both through experiments and through simulation - to reduce the stray light only by 9 %. We may therefore try to adopt a more complete representation of the lighting conditions, such as that of Basri and Jacobs [19]. In addition, we expect that our large-scale surface reconstructions (image width close to 10 cm or larger) may improve through the adoption of the interreflection removal ideas presented by Liao et al. [20]. They estimate the impact of interreflections through illuminating the target with lights of different colors, which is readily possible with our RGB leds.

Encouraged by the observed dependences of paper surface topographies on illumination configuration and wavelength, further tests will be run with paper samples using the different colored lights. Finally, polarized light - combined with a polarizer in front of the camera objective - will be tested because it offers a straightforward way of blocking specular reflections. This has been utilized in paper research by, e.g., Hansson and Johansson [21].

5. CONCLUSIONS

We have presented our photometric stereo based measurement system that has been designed for versatile surface topography measurements of planar targets. Thanks to the travelling table, movable lights and stable construction, our system is ideal for experimenting on the effects that occur on the surfaces of, e.g., fibrous materials, when observed in the scale from a few micrometers to a few millimeters. We have been able to align a reference surface topography map of an aluminium oxide test piece with topography maps estimated with the photometric stereo based system. We have also examined the surfaces of paper samples under versatile lighting directions and light colors. The results demonstrate the dependence of the surface reconstructions on resolution, lighting conditions, and surface roughness.

ACKNOWLEDGMENTS

The authors would like to acknowledge Jarmo Verho and Juha Koljonen (TUT) for their contribution in the design and

implementation of several electronic and mechanical parts of the measurement system. The funding from the Academy of Finland (Dec. No. 258124) is gratefully acknowledged.

REFERENCES

[1] R. J. Woodham, "Photometric method for determining surface orientation from multiple images", *Optical Engineering*, vol. 19, n° 1, pp. 139-144, Feb. 1980.

[2] H. D. Tagare and R. J. P. deFigueiredo, "A theory of photometric stereo for a class of diffuse non-lambertian surfaces", *IEEE Trans. Pattern Analysis and Machine Intelligence*, vol. 13, n° 2, pp. 133-152, Feb. 1991.

[3] A. S. Georghiades, "Incorporating the Torrance and Sparrow Model of reflectance in un-calibrated photometric stereo", *Int. Conf. Computer Vision*, pp. 816–823, Nice, France, Oct. 2003.

[4] V. Argyriou and M. Petrou, "Recursive photometric stereo when multiple shadows and highlights are present", *IEEE Conf. Computer Vision and Pattern Recognition*, pp. 1-6, Anchorage, Alaska, USA, June 2008.

[5] N. Alldrin, T. Zickler and D. Kriegman, "Photometric stereo with non-parametric and spatially-varying reflectance", *IEEE Conf. Computer Vision and Pattern Recognition*, pp. 1-8, Anchorage, Alaska, USA, June 2008.

[6] V. Argyriou, M. Petrou and S. Barsky, "Photometric stereo with an arbitrary number of illuminants", *Computer Vision and Image Understanding*, vol. 114, n° 8, pp. 887-900, August 2010.

[7] S. Ikehata, D. Wipf, Y. Matsushita and K. Aizawa, "Photometric stereo using sparse Bayesian regression for general diffuse surfaces", *IEEE Trans. Pattern Analysis and Machine Intelligence*, vol. 36, n° 9, pp. 1816-1831, Sept. 2014.

[8] G. G. Barros and P.-Å. Johansson, "Prediction of UnCovered Area occurrence in flexography based on topography – A feasibility study", *Nordic Pulp Paper Res. J.*, vol. 21, n° 2, pp. 172-179, 2006.

[9] M. Mettänen, *Measurement of print quality: Joint statistical analysis of paper topography and print defects*, PhD thesis, Tampere University of Technology, Tampere, 2010. http://urn.fi/URN:NBN:fi:tty-201011231371

[10] L. Mattsson and P. Wågberg, "Assessment of surface finish on bulk scattering materials: a comparison between optical laser stylus and mechanical stylus profilometers", *Precision Engineering*, vol. 15, n° 3, pp. 141-149, July 1993.

[11] A. Sohaib, A. R. Farooq, G. A. Atkinson, L. N. Smith, M. L. Smith and R. Warr, "*In vivo* measurement of skin microrelief using photometric stereo in the presence of interreflections", *J. Opt. Soc. Am. A*, vol. 30, n° 3, pp. 278-286, March 2013.

[12] H. Granberg, J. Jensen and L. Mattsson, "Forward scattering of fiber-containing surfaces studied by 3-D reflectance distribution simulations and measurements", *Optical Engineering*, vol. 42, n° 8, pp. 2384-2390, Aug. 2003.

[13] S. Tominaga, "Surface identification using the dichromatic reflection model", *IEEE Trans. Pattern Analysis and Machine Intelligence*, vol. 13, n° 7, pp. 658-670, July 1991.

[14] J. Sun, M. Smith, L. Smith and A. Farooq, "Illumination compensation for nominally planar surface recovery", *IET Computer Vision*, vol. 6, n° 5, pp. 371-377, Sept. 2012.

[15] R. T. Frankot and R. Chellappa, "A method for enforcing integrability in shape from shading algorithms", *IEEE Trans. Pattern Analysis and Machine Intelligence*, vol. 10, n° 4, pp. 439-451, April 1988.

[16] R. Hartley and A. Zisserman, Multiple View Geometry in Computer Vision, 2nd Ed., Cambridge University Press, 2003.

[17] M. Lähdekorpi, H. Ihalainen and R. Ritala, "Using image registration and alignment to compare alternative 2D measurements", XVIII IMEKO World Congress, Rio de Janeiro, Brazil, September 2006.

[18] N. Pauler, Paper Optics, Chp 4 in *Paper Physics* (K. Niskanen ed.), Paper and Timber, 2012.

[19] R. Basri and D. Jacobs, "Photometric stereo with general, unknown lighting", *IEEE Conf. Computer Vision and Pattern Recognition*, vol. 2, pp. II-374-II-381, Kauai, Hawaii, Dec. 2001.

[20] M. Liao, X. Huang and R. Yang, "Interreflection removal for photometric stereo by using spectrum-dependent albedo", *IEEE Conf. Computer Vision and Pattern Recognition*, pp. 689-696, Colorado Springs, USA, June 2011.

[21] P. Hansson and P.-Å. Johansson, "Topography and reflectance analysis of paper surfaces using a photometric stereo method", *Optical Engineering*, vol. 39, n° 9, pp. 2555-2561, Sept. 2000.